Chapter 5

Adsorption using ATA

5.1 Adsorption of Cu^{2+}, Ni^{2+} and Zn^{2+} ions by ATA

Copper, nickel and zinc contamination are caused by electroplating, metal processing, mining, petroleum refining, pulp and paper mills, steel and iron smelting units [315]. Various traditional heavy metal removal techniques have been used to treat the industrial effluent. Some of the approaches include chemical precipitation [316], ion exchange [99], electrochemical process [317], membrane technology [318] and activated carbon adsorption [319]. But these methods have their disadvantages, namely lack of efficiency, higher power demands and extremely expensive, particularly while handling a low concentration of heavy metal present in significant quantities of wastewater.

Adsorption has been observed to be inexpensive and more effective than other chemical techniques in the recent years. Low cost, significant decrease in chemical and biological sludge production and high efficiency are the key characteristics of the adsorption process. The binding of metal ions on the surface of adsorbents relies on the chemical characteristics of metal ions (charge and size), type of biomass and environmental conditions (pH, temperature) [56]. Natural materials which are abundantly available and perhaps agro-waste are potential inexpensive adsorbent. Adsorption of heavy metals using activated carbon is a quick and efficient process widely accepted in the industry. Additional chemicals may also be required to improve the effectiveness of adsorption in wastewater. Due

to these limitations, a more efficient approach must be taken that should not only be inexpensive but also more productive. Adsorption based on natural resources demonstrates a more efficient metal scavenging process with low operating costs. It does not involve any additional chemistry, biological restoration and recovery process of metals. The purpose of the present study is to use *Azadirachta indica* twig ash (ATA), left after domestic use to treat contaminated water containing Cu^{2+}, Ni^{2+} and Zn^{2+} ions.

In India, some of the major *Azadirachta indica* producing states are Uttar Pradesh, Tamil Nadu, Karnataka, Madhya Pradesh, Maharashtra, Andhra Pradesh and Gujarat [320]. It has enormous potential in the field of pesticide control, protection of the environment and medicine. This is one of the most studied trees in the world and is the most promising tree of the twenty-first century [177]. *Azadirachta indica* products have water purification capability. *Azadirachta indica* twigs have antiseptic properties. *Azadirachta indica* has now gained international popularity as natives of all countries are inclined towards green technology. *Azadirachta indica* products do not harm humans or livestock and do not have a residual effect on farm products. The total number of *Azadirachta indica* trees in India is about 18 million [178].

In the present study, the chosen adsorbent is inexpensive, eco-friendly, easily available and does not lead to any contamination in the environment. Previously, *Azadirachta indica* seeds, bark and leaves have been rigorously used as an adsorbent by various researchers [321], but very scarce information is available regarding the use of ATA in removing heavy metals from contaminated water. The present investigation aimed at the usage of ATA for removal of Cu^{2+}, Ni^{2+} and Zn^{2+} ions from wastewater. In addition, physico-chemical characterization of ATA, adsorption dynamics, optimization study, isotherm, kinetic, mechanistic and thermodynamic correlations were studied in detail in order to understand the basic mechanism of metal ions on the ATA surface. ANN tool of MATLAB has been used to compare the experimental result with the predicted outcome. Finally, a comparative analysis of ATA with other adsorbents reported by other researchers has also been presented.

5.2 Results and Discussion

5.2.1 Characterization

5.2.1.1 SEM-EDX

SEM images of the ATA before and after adsorption of ternary metal ions have been shown in Figures 5.1 and 5.2, respectively.

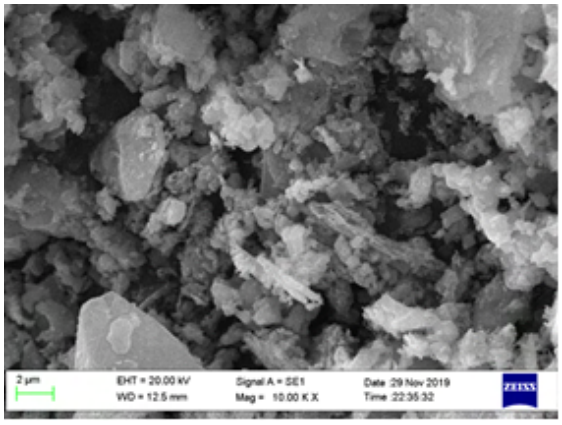

Figure 5.1: SEM of ATA before adsorption of ternary metal ions

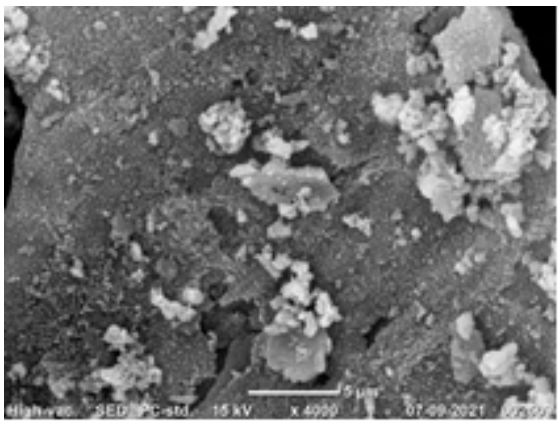

Figure 5.2: SEM of ATA after adsorption of ternary metal ions

The micrographs showed that small particles formed were not regular in shape and size [322]. Similarly, Al Moharbi et al., 2020 [323] reported the irregular shape and size of the particles of *Azadirachta indica* leaf powder while removing copper ions from industrial effluent. Figure 5.1 demonstrates that the ATA seems to have heterogeneous and porous surface. Similar characteristics of *Azadirachta indica* bark like porous and irregular surface were observed by Naiya et al., 2009 [324] while removing Zn^{2+} and Cd^{2+} ions from

aqueous solutions. *Azadirachta indica* twig is a cellulose-based substance consisting of organic compounds like tannins and lignin [324]. Figure 5.1 shows that the ash is made up of fine particles (before adsorption), that does not possess regular, fixed shape and size. After adsorption, heterostructure showed agglomerated appearance. (Figure 5.2). The findings of EDX showed that ATA primarily consisted of C and O and minimal quantity of Al, Mg, Ca, Na, Si, N, K, P and S (Figure 5.3a) [325].

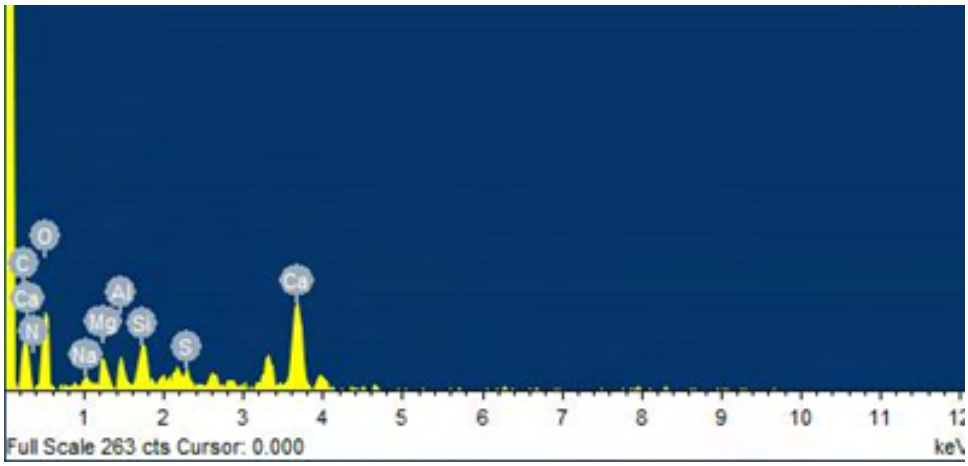

(a) EDX of ATA before adsorption of ternary metal ions

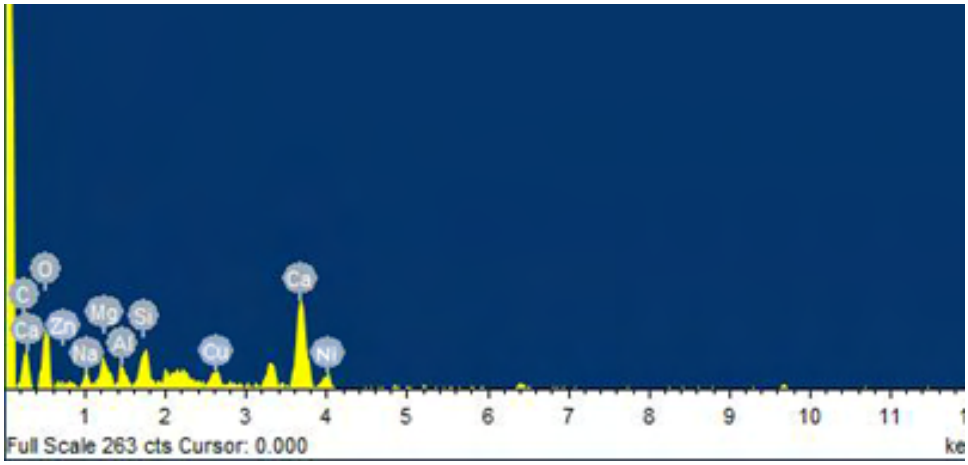

(b) EDX of ATA after adsorption of ternary metal ions

Figure 5.3: EDX of ATA

The EDX of ATA before and after the adsorption (Figures 5.3a and 5.3b) validated that ternary metal ions were adsorbed on ATA surface, thereby making it a suitable adsorbent for removing contamination from water. Ang et al., 2013 [326] conducted research on neem leaf powder for removal of copper ions and similar to the present study, EDX showed the presence of carbon, oxygen, magnesium, phosphorus, sulphur, potassium and

calcium. Sulaiman, 2015 [325] utilized neem leaf powder to remove Cu^{2+} ions from contaminated water and discovered that EDX clearly indicates that neem leaf powder is mostly composed of carbon and oxygen, with trace amounts of calcium, magnesium, potassium, phosphorus, and sulphur. The findings of Sulaiman (2015) are consistent with those of the present study and Ang et al., 2013 [326].

5.2.1.2 FTIR

The presence of several functional groups was identified in the FTIR spectra of ATA as shown in Figure 5.4. The BA and AA legend in graph depict before adsorption and after adsorption, respectively.

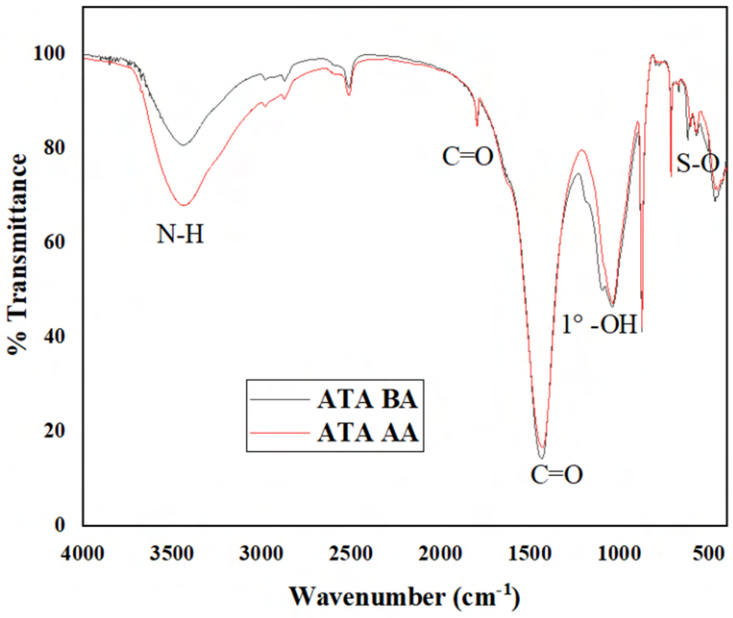

Figure 5.4: FTIR Spectrum of ATA before and after adsorption of ternary metal ions

On comparing unloaded to metal loaded ATA, the wavenumber of dominant peaks associated with the loaded metal were observed to be changed. The change in wavenumber revealed metal binding on the surface of ATA. O-H stretching of the carboxylic groups was found to shift explicitly after adsorption from wavenumber 2986.32 cm^{-1} to 2978.93 cm^{-1}. Such a significant shift (7.32 cm^{-1}) in the band showed high metal-binding potential of O-H stretching present in the ATA. For the amine group, the wavenumber for

N-H stretching was changed from 3447.60 cm^{-1} to 3436.93 cm^{-1}after adsorption. The shift in N-H stretching of the amine group was correlated with metal ions adsorption. The C=O stretching of syringaldehyde was confirmed by the peak at 1795.34 cm^{-1} which changed to 1794.21 cm^{-1} after metal loading. Similar changes were observed by Popuri et al., 2007 [327] in metal loaded raw *Azadirachta indica* sawdust and metal loaded acid treated *Azadirachta indica* sawdust while removing copper and nickel from aqueous solutions. The 6-membered cyclic ether group of cellulose in the spectra was obtained at 1096.03 cm^{-1} and that disappeared after adsorption [327]. The wavenumber 1044.32 cm^{-1} represented the primary -OH group. The S-O stretching in the sulphonate group prior to adsorption was at 618.95 cm^{-1}, but it disappeared after adsorption. The absence of certain peaks showed that the sample no longer contains such chemical bonds. It is worth noting that FTIR findings did not include any quantitative analysis or the degree of affinity to the metal of the adsorbent functional groups.

Findings proposed are the only probability to couple the metal species with the adsorbent functional group [324]. Naiya et al., 2009 [324] reported the presence of several functional groups such as carboxylic acid, amine, amino, amide and sulphonate groups on the *Azadirachta indica* bark and similar groups were found in the present study. Al Moharbi et al., 2020 [323] mentioned that niacin, proline, glutamic acid, aspartic acid, glutamine, tyrosine and alanine on *Azadirachta indica* leaf powder might be associated with surface charge and various negatively charged functional groups.

5.2.1.3 XRD

X-ray diffraction analysis was performed to assess the crystallinity of ATA (Figure 5.5a and 5.5b).

The pattern was examined at an angle of 10 to 80º (2θ). The degree of crystallinity was identified by comparing the areas of crystalline peaks and amorphous curves. The XRD graph of ATA revealed that the substance is partly amorphous and should find application as an adsorbent [220], [328]. Table 5.1 showed that the ATA was less crystalline (41.6%) or more amorphous (58.4%). This helps in enhancing the adsorption efficiency

of any adsorbent. Uilizing Scherrer equation, the FWHM of the ATA (Table 5.1) has been calculated and utilized to determine the crystal size of the ATA.

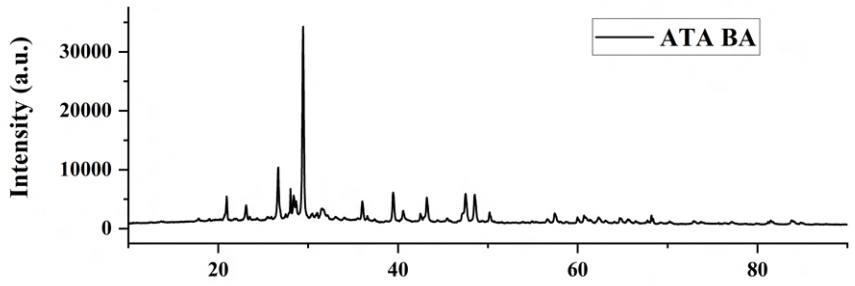

(a) Before adsorption

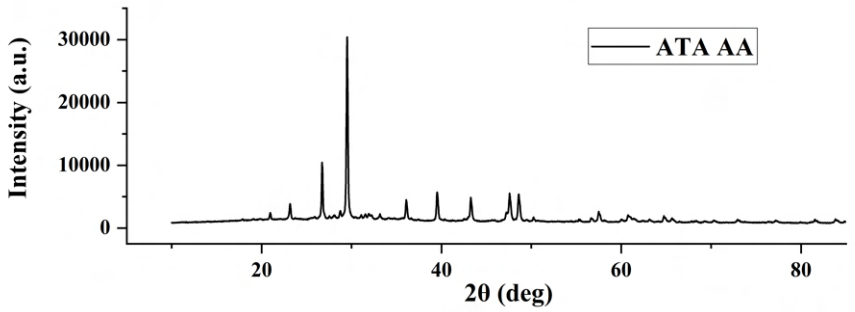

(b) After adsorption

Figure 5.5: XRD of ATA before and after adsorption of ternary metal ions

Table 5.1: X-Ray Diffraction analysis of ATA

(a) Before adsorption

Area	FWHM	Crystallinity
1671.01	0.18	41.6%
1608.92	0.27	
3208.52	0.21	
9213.89	0.19	
1743.94	0.71	
1507.14	0.25	
1920.66	0.24	
1197.45	0.33	
1755.43	0.25	

(b) After adsorption

Area	FWHM	Crystallinity
926.72	0.27	41.14%
1424	0.23	
2565.03	0.16	
7603.19	0.19	
1538.82	0.24	
2147.39	0.24	
1801.34	0.24	
1969.91	0.29	
1776.87	0.28	

5.2.1.4 BET Surface Area

The BET method was used to calculate the ATA's surface area. This is the most essential aspect in determining the adsorption capacity of an adsorbent. It is commonly acknowledged that adsorption becomes more promising when there are more active sites on the surface [329], [330]. In the present study, the BET surface area, average pore diameter and total pore volume were found to be 71.35 m^2/g, 10.07 nm and 0.193 cm^3/g, respectively which indicated that ATA could be a better adsorbent. Using BET analysis, Sadare and Daramola, 2020 [331] observed that neem leaf powder has a surface area of 73.21 m^2/g when they studied its efficacy for desulfurization of petroleum distillate.

5.2.1.5 Proximate and Ultimate Analysis

The proximate analysis of ATA quantified 55.22% fixed carbon, 8.51% moisture, 14.78% ash and 21.49% volatile matter. The lower ash content in ATA indicated that adsorbent was properly prepared. The ultimate analysis of ATA showed 38.47% C, 1.89% H, 49.21% O, 10.43% N.

Similarly, Otache and Godwin, 2017 [332] investigated the proximate and mineral compositions of neem leaves and discovered that the proximate compositions ranged from 12.10 to 14.30 % for moisture, 3.88 to 4.03% for ash, 1.22 to 4.04% for protein, 2.89 to 3.18% for fat and 9.25 to 10.86% for fiber.

5.2.1.6 Bulk Density

The bulk density affects metal ion adsorption. The reduction in bulk density increases metal ion adsorption. It was reported by Gopalakrishnan et al., 2009 [56] that smaller is the particle size of the adsorbent, higher is the adsorption. The lower value of bulk density suggests that particles are fine in nature. The bulk density of ATA was calculated as 0.47 $g/cm^{3.}$ A suitable adsorbent has a lower bulk density value. The occurrence of micropores in the structure was reported through bulk density [333]. The apparent bulk density of the ATA was in the range of acceptable limit recommended by ASTM, i.e., 0.42 - 0.52 g/cm^3 [334]. Similarly, Balami et al., 2014 [335] investigated the physical parameters

of neem seeds and kernels that are relevant for the design of processing machinery and discovered a bulk density of 0.39 g/cm^3.

5.2.2 pH_{ZPC}

The pH_{zpc} of ATA is shown in Figure 5.6.

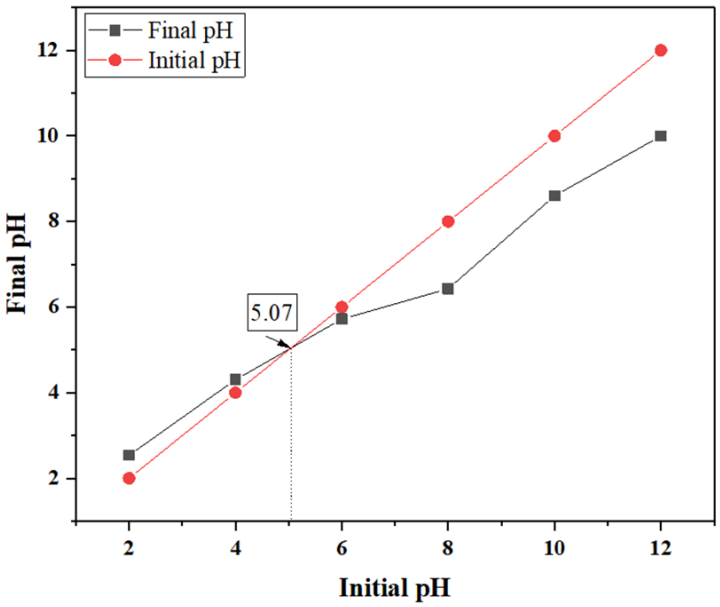

Figure 5.6: pH_{zpc} of ATA

The point where two curves intersect is the zero-point charge pH of the sample. The pH_{zpc} of ATA was found to be 5.07 in the present study. It means above this value; the surface will be negatively charged. Sahmoune and Yeddou, 2016 [336] and Georgiadis et al., 2013 [337] reported that adsorption of cationic metal ions is favored at pH > pH_{zpc}, due to the existence of functional groups like OH^-, COO^- groups. Similar results were found in the present study.

5.2.3 Adsorption Dynamics

In this study, values of the film (2.13×10^{-12}, 5.17×10^{-12}, 3.43×10^{-11} cm^2 sec^{-1}) and pore diffusivity (3.70×10^{-13}, 4.44×10^{-13}, 5.55×10^{-13} cm^2 sec^{-1}) coefficients for Cu^{2+}, Ni^{2+} and Zn^{2+} ions, respectively revealed that the mechanism of adsorption relies on pore diffusion. The values of dimensionless numbers φ, λ and N_k were shown in Table 5.2.

Table 5.2: Value of dimensionless numbers for ternary metal ions

Dimensionless numbers	φ	λ	N_k
Cu^{2+}	65.59	0.0002	27
Ni^{2+}	61.51	0.0008	29
ZN^{2+}	60.05	0.0009	34

The value of N_k fell between 10^1 and 10^4, which interpreted that adsorption dynamics was controlled by diffusion. The value of φ and λ were in the range of 10^{-2} to 10^4 and 10^{-12} to 10^8, which showed extensive ATA surface coverage during adsorption with reduced surface tension [212].

5.2.4 ANN Modeling

MATLAB has been used for ANN computation to predict adsorption of Cu^{2+}, Ni^{2+} and Zn^{2+} ions in solution.

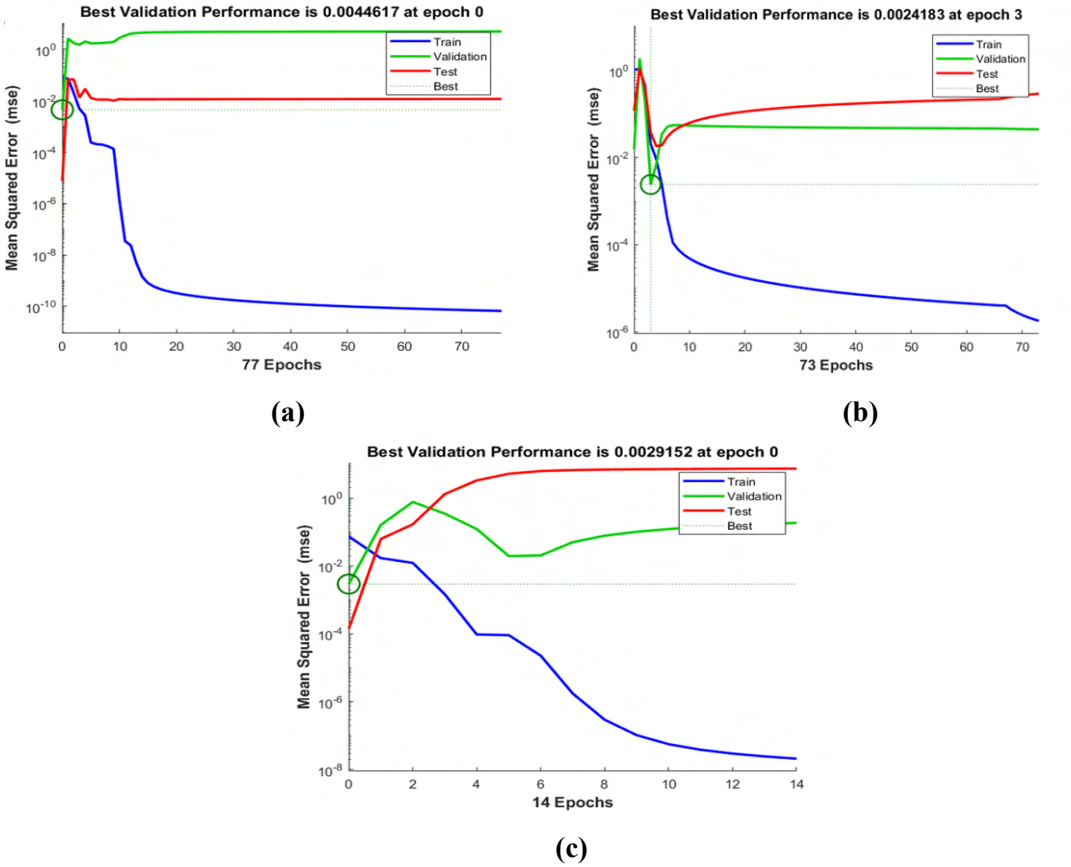

Figure 5.7: Performance between number of epochs and MSE for prediction of (a) Cu^{2+}, (b) Ni^{2+} and (c) Zn^{2+} ions removal using ATA as adsorbent

Figure 5.7 demonstrates MSE of the ANN model which was developed by using the L-M algorithm training, testing and validation of data sets. The lowest MSE at epoch (0, 3, 0 for Cu^{2+}, Ni^{2+} and Zn^{2+} ions) coupled and highest validation performance in ten neurons at 0.0044, 0.0024 and 0.0029 for Cu^{2+}, Ni^{2+} and Zn^{2+} ions,respectively. The L-M Algorithm was evaluated by using regression plot by training, validation of test data sets while matching the expected output with experimental results (Figure 5.8).The analysis of predicted and test results produced a high coefficient of correlation (R^2 = 0.99) (Figure 5.8), which implies that the proposed model has been able to predict the efficacy of adsorption appropriately [231].

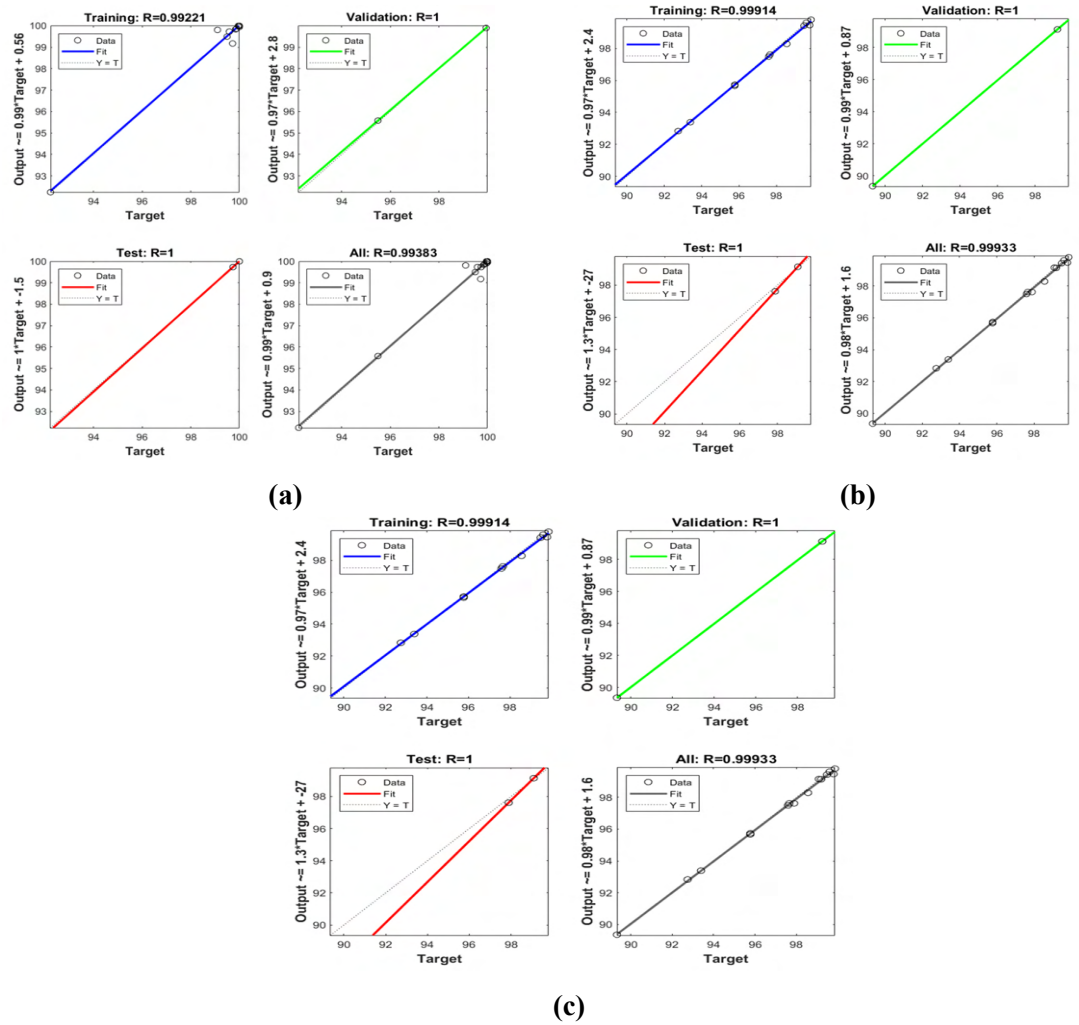

Figure 5.8: Regression plot for prediction of (a) Cu^{2+}, (b) Ni^{2+} and (c) Zn^{2+} ions removal using ATA as adsorbent

Correlation plots between experimental and predicted values are shown in Figure 5.9 for

further verification of result.

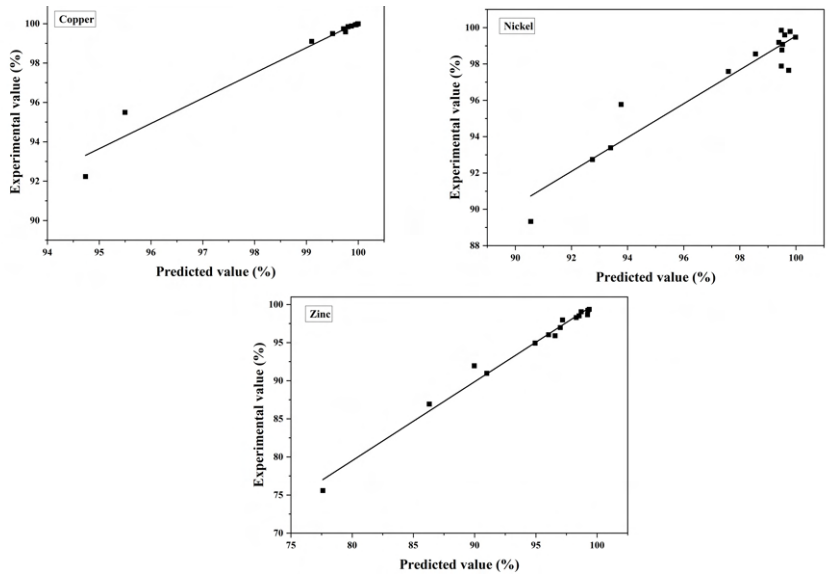

Figure 5.9: Correlation plot for the experimental and ANN predicted values for ternary metal ions removal using ATA as adsorbent

The results showed a deviation of 0.16% for Cu^{2+}, 0.09% for Ni^{2+} and 0.08 % for Zn^{2+} between the experimental and the ANN predicted values. The prediction model showed that the ANN model was able to predict the percentage removal of Cu^{2+}, Ni^{2+} and Zn^{2+} ions by ATA with $R^2 = 0.99$.

5.2.5 Adsorption Kinetics

Kinetic models were used to test the experimental data to assess the mechanism of adsorption of ternary metal ions on ATA and possible rate-controlling steps, like mass transport and chemical reactions. Figure 5.10 and Table 5.3 displays the results of adsorption kinetics.

In the present investigation, three kinetic models have been used to study the adsorption kinetics of ternary metal ions. Experimental results for the best linear fit were checked to find out the parameters for each kinetic model. Results showed that the adsorption of ternary metal ions on ATA were better interpreted by the PSO kinetic model with a high regression coefficient as shown in Table 5.3. On the other hand, IPD model showed significant closeness to the PSO model based on the value of the R^2. These results were

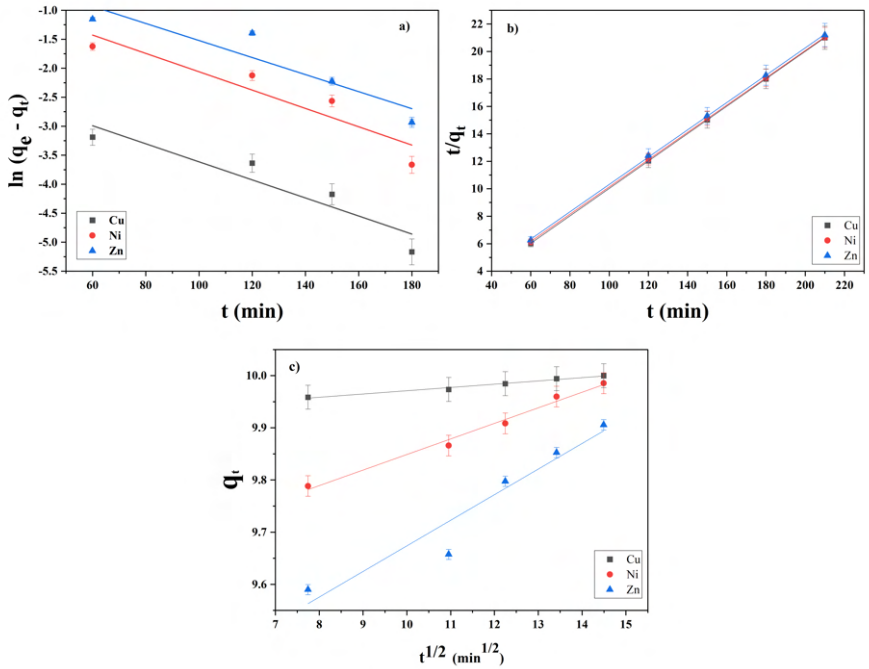

Figure 5.10: (a) PFO, (b) PSO and (c) IPD model for ATA as adsorbent

Table 5.3: Adsorption kinetic model parameters for ATA as adsorbent

Kinetic Parameter		PFO		PSO		IPD	
		q_e (mg/g)	k_1 min^{-1}	q_e (mg/g)	k_2 (g/mg. min)	k_p (mg/g. min)	C (mg/g)
Value	Cu	0.13	0.02	10.02	0.23	0.01	9.90
	Ni	0.62	0.02	10.07	0.05	0.03	9.55
	Zn	0.95	0.01	10.06	0.03	0.05	9.20
R^2	Cu	0.88		1.00		0.98	
	Ni	0.87		0.99		0.99	
	Zn	0.86		0.99		0.93	
SSE	Cu	0.26		0.00002		1.88×10^{-5}	
	Ni	0.30		0.01		3.2×10^{-4}	
	Zn	0.28		0.02		0.01	
χ^2	Cu	0.13		0.00001		0.00001	
	Ni	0.15		0.003		0.0002	
	Zn	0.14		0.01		0.003	

in accordance with Malik et al., 2014 [338] demonstrated the feasibility of PSO kinetic model when evaluating adsorption of copper and zinc on *Azadirachta indica* leaf. IPD equation plot of q_t *vs* $t^{1/2}$ suggested that the process is consisting of more than one adsorption mechanism as shown in Figure 5.3

From these modeling results, it is observed that adsorption of metal ions was adjusted to the heterogeneous diffusion model. The findings of the present study showed that as long as the material is multilayered, the kinetics of heavy metal adsorption almost matches to the PSO kinetic model.

5.2.6 Adsorption Isotherm

Langmuir, Freundlich and D-R isotherm were investigated in the present study (Figure 5.11).

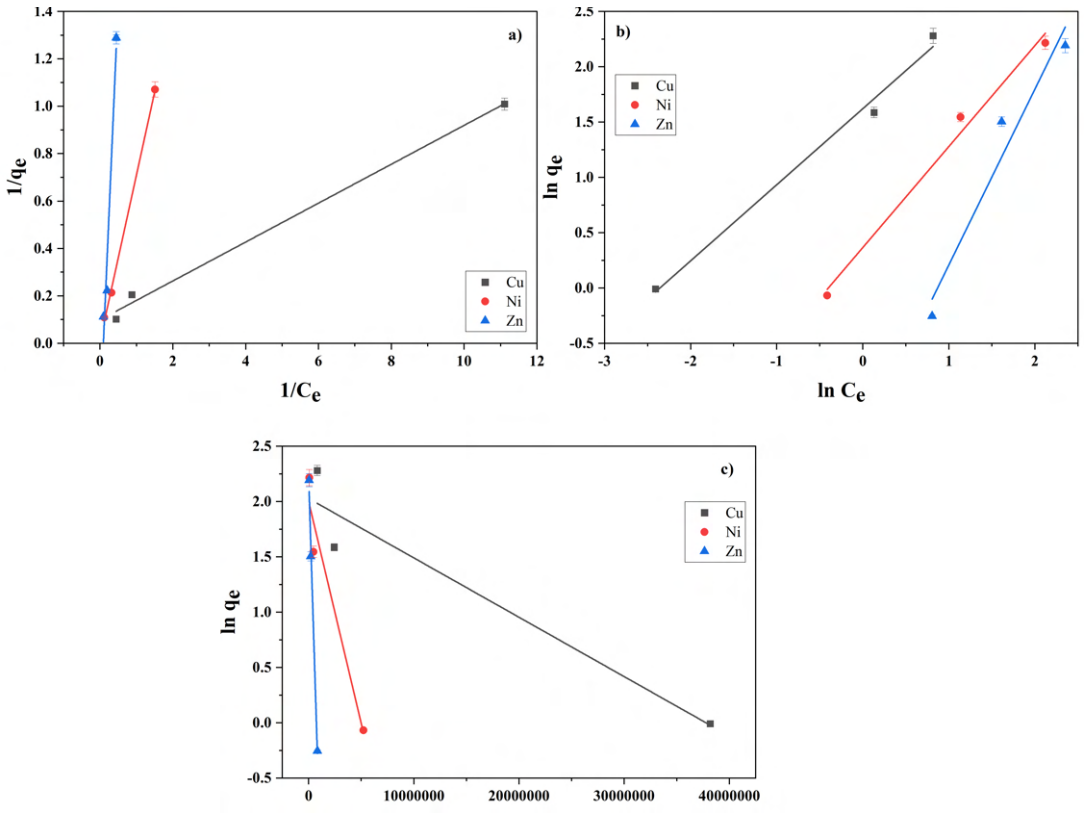

Figure 5.11: a) Langmuir, b) Freundlich and c) D-R isotherm models for ATA as adsorbent

The calculated isotherm constants, regression coefficients, Chi-square and sum of the square of errors (SSE) for each isotherm have been shown in Table 5.4.

Table 5.4: Adsorption isotherm model parameters for ATA as adsorbent

Isotherm		**Langmuir**		**Freundlich**		**D-R**		
Parameter		**q_m (mg/g)**	**K_F (L/mg)**	**n**	**K_L (L/mg)**	**β**	**E (J/mol)**	**q_m (mg/g)**
Value	**Cu**	10.10	1.20	1.45	1.10	5.36×10^{-8}	4319.34	7.61
	Ni	125	0.01	1.10	2.17	4.01×10^{-7}	1579.16	7.38
	Zn	3.12	0.09	0.63	5.46	3×10^{-6}	576.39	9.39
R^2	**Cu**	0.99		0.99		0.93		
	Ni	0.99		0.99		0.95		
	Zn	0.96		0.95		0.99		
SSE	**Cu**	0.002		0.03		0.18		
	Ni	6.9×10^{-7}		0.03		0.13		
	Zn	0.04		0.16		0.03		
χ^2	**Cu**	0.001		0.01		0.09		
	Ni	3.45×10^{-7}		0.02		0.07		
	Zn	0.02		0.08		0.02		

Higher values of the correlation coefficient (R^2) and lower values of chi-square and SSE suggested that Langmuir isotherm model was the best one for ternary metal ions adsorption. The main characteristic feature of Langmuir was R_L (separation factor) which determines the favorability of adsorption as a dimensionless separation factor. In the present work, the R_L value was < 1 (0.012 for Cu^{2+}, 0.0001 for Ni^{2+} and 0.0009 for Zn^{2+}) which shows favorable adsorption [277]. In D-R isotherm, 'E' was less than 8 kJ/mol that indicated the role of physical adsorption on the surface of ATA (Figure 5.4) [278]. The value of 'n' in Freundlich isotherm gives an indication of favorable adsorption as shown in Table 5.4 [279], [339]. These findings were consistent with other researchers who also considered Langmuir model to be the best-fitted when they studied the adsorption of metal ions on *Azadirachta indica*-based adsorbents [224]. Barros et al., 2008 [280] reported similar results during the removal of Cu^{2+}, Ni^{2+} and Zn^{2+} ions using *Azadirachta indica* leaf powder.

5.2.7 Thermodynamics Study

Thermodynamic parameters were calculated by plotting the curve between ln K_d and 1/T (Figure 5.12).

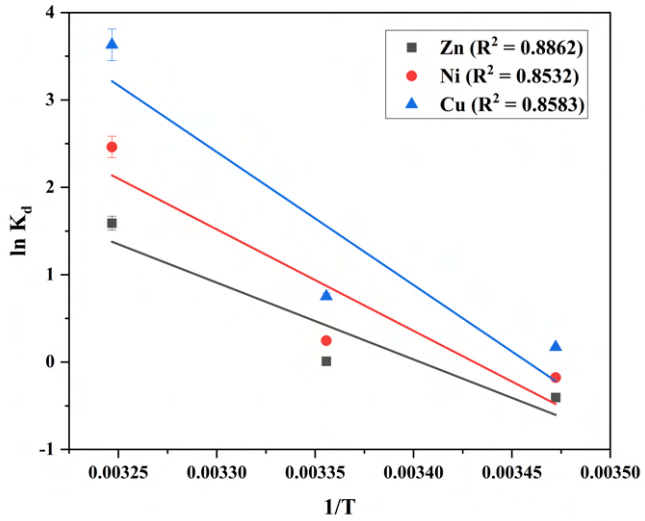

Figure 5.12: Plot of ln K_d vs. 1/T for ATA as adsorbent

Table 5.5 displays the thermodynamic parameter profiling of Cu^{2+}, Ni^{2+} and Zn^{2+} ions adsorption on ATA.

Table 5.5: Thermodynamic parameters for ATA as adsorbent

Temperature (K)		**298**	**308**	**313**
ΔG (J/mol) (Experimental)	**Cu**	-411.82	-1862	-9299.9
	Ni	424.94	-608.07	-6302.7
	Zn	972.87	-24.07	-4069.6
ΔS (J/mol K)	**Cu**	437.65		
	Ni	331.15		
	Zn	248.71		
ΔH (kJ/mol)	**Cu**	126579.2		
	Ni	96527.95		
	Zn	73076.65		

The negative value of ΔG implies the spontaneous nature for adsorption of ternary metal ions onto ATA [274]. The findings were consistent with Febriana et al., 2010 [340] who

notified the similar endothermic adsorption copper ions om of *Azadirachta indica* leaf. Moreover, the value of ΔG was found to be < + 20 kJ/mol, which ruled out electrostatic interaction possibilities between active sites of ATA and metal ions [283]. In this study, positive value of ΔH (Table 5.5) indicated the endothermic adsorption of ternary metal ions [284]. This may be attributed to the distribution of the Cu^{2+}, Ni^{2+} and Zn^{2+} ions hydration spheres on ATA surface before adsorption activity. The dehydration process required energy and was therefore, favored at higher temperature range [284], [285]. The positive value of ΔS (Table 5.5) leads to improved randomness at the solid-aqueous interface with somewhat structural changes in ATA after interaction with metal ions [274].

5.2.8 Optimization Study

5.2.8.1 Effect of pH

The effects of pH on the adsorption of ternary metal ions were investigated in the pH range of 3.0 to 11.0 (Figure 5.13).

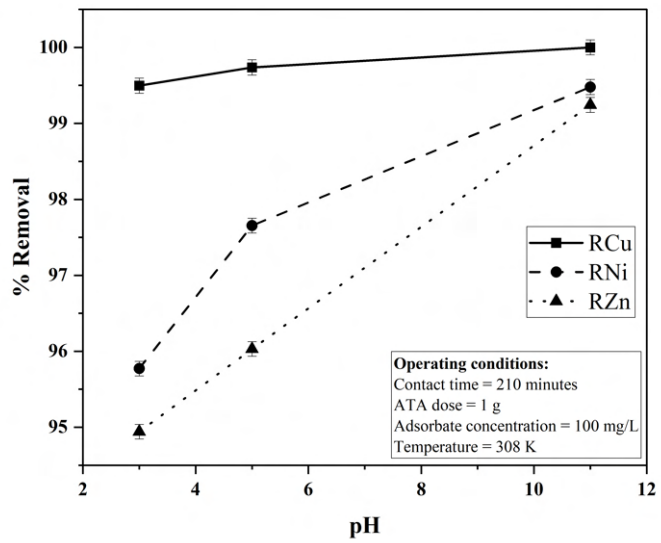

Figure 5.13: Effect of pH on percentage removal of ternary metal ions using ATA

Experiments were performed at the initial metal ions concentration of 100 mg/L for 210 minutes with an ATA mass of 1 g at 35°C. The rise in pH from 2.0 to 6.0 contributed to the rise in the uptake of ternary metal ions and maximum adsorption was reported at pH 6. At pH values above 6, precipitates of Cu^{2+}, Ni^{2+} and Zn^{2+} ions were obtained

due to the high OH^- ion concentration. The overall surface charge at low pH values are positive and hinder the path of metal cations with positive charge [324]. The ATA surface being negatively charged showed an increase in adsorption of Cu^{2+}, Ni^{2+} and Zn^{2+} ions by increasing electrostatic attraction between positively charged ions and negatively charged ATA. Similar findings were reported by Febriana et al., 2010 [340] while removing copper ions using *Azadirachta indica* leaf and Naiya et al., 2009 [324] during removal of Zn^{2+} and Cd^{2+} ions from aqueous solutions with sawdust and *Azadirachta indica* bark. Thus, optimum pH was taken as 6 for further experiments.

5.2.8.2 Effect of ATA Dose

The adsorption of ternary metal ions in the ATA have been investigated at 35°C with ATA dose ranging from 1 g to 2 g while maintaining constant volume (100 ml) and metal ion solution concentration (100 mg/L). The batch adsorption study was conducted for 210 minutes at pH 6. Figure 5.14 shows the result.

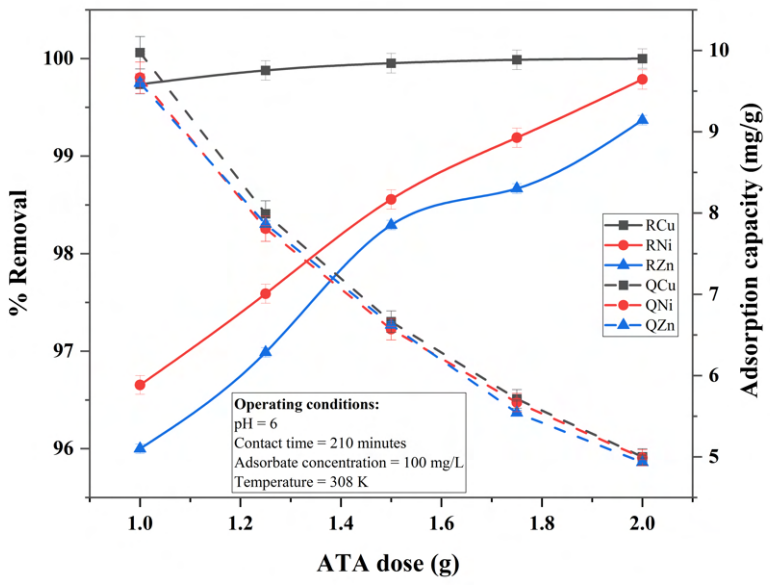

Figure 5.14: Effect of ATA dose on percentage removal of ternary metal ions and adsorption capacity of ATA

It is clear from Figure 5.14 that the percentage removal of Cu^{2+}, Ni^{2+} and Zn^{2+} ions increased quickly with the increase in the dose of ATA. This may be attributed to the increased availability of exchangeable sites with higher ash content [324]. However, the

adsorption capacity decreases from 9.97 to 5 mg/g and 9.66 to 4.98 mg/g and 9.6 to 4.93 mg/g for Cu^{2+}, Ni^{2+} and Zn^{2+} ions, respectively from 1 to 2 g dose. The reduction in adsorption capacities with increased adsorbent dose is primarily due to unsaturation of adsorption sites present on the surface of ATA [341]. Rasheed et al., 2014 [342] observed similar findings during adsorption of Cu^{2+} on *Azadirachta indica* leaf powder as it is composed of incredibly fine organic particle that agglomerates at high doses, which blocks interior active sites. This leads to low metal uptake and decreased copper removal at higher doses. For all experiments, 1 g was taken as the optimum ATA dose.

5.2.8.3 Effect of Initial Concentration

The effect of initial adsorbate concentration was tested using various initial ternary metal ions concentrations (10-100 mg/l) at 35 °C temperature, 210 minutes contact time, pH 6 and 1 g ATA dose. The adsorption capacity of ATA increases with the increase in initial metal ion concentration (0.991 - 9.7736 mg/g of Cu^{2+}, 0.9339 - 9.1654 mg/g of Ni^{2+}, and 0.776 - 8.948 mg/g of Zn^{2+}) as shown in Figure 5.15 . Increase in initial concentration of metal ions from 10 to 100 mg/L helps to reduce mass transfer resistance between the adsorbent and bulk fluid phases, thus increasing metal ion uptake [222], [343]. It is evident from Figure 5.15 that adsorption capacity increased as adsorbate concentration increased, while percentage removal decreased.

At low initial meal ion concentrations, the surface area and adsorption sites were abundant, and the Cu^{2+}, Ni^{2+} and Zn^{2+} ions were easily adsorbed and removed. Since the total accessible adsorption sites are limited at higher initial solution concentrations, the percentage removal of Cu^{2+}, Ni^{2+} and Zn^{2+} ions decreased. In addition, an increase in metal ion concentrations increases the number of collisions between metal ions and adsorbents, leading to enhanced adsorption [344]. Malik et al., 2014 [338] utilized *Azadirachta indica* leaf for removal of copper and zinc ions and found that adsorption sites picked up the available metal more easily at low concentrations. However, at higher concentrations, metal ions diffuse by intraparticle diffusion into the biomass surface and hydrolyzed ions can diffuse at a slower rate. Thus, 100 mg/L was observed as the optimum concentration

that was considered for further experimental work.

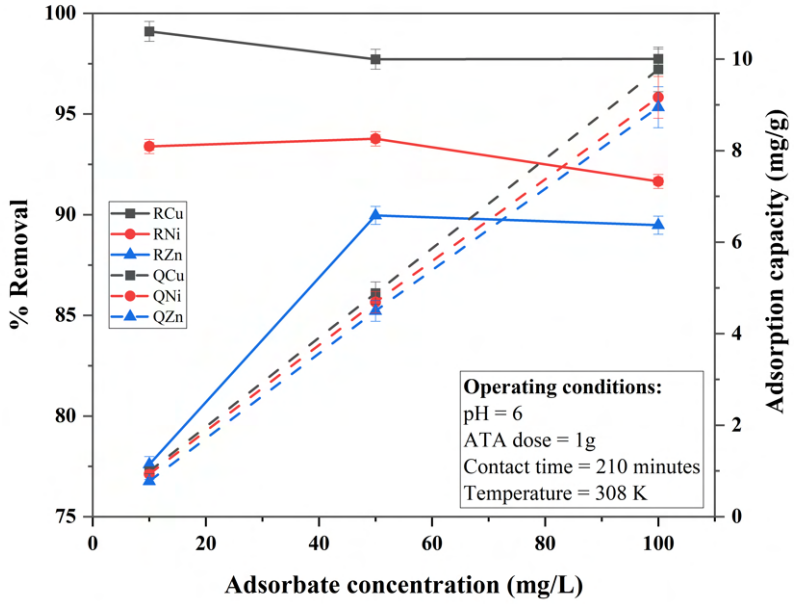

Figure 5.15: Effect of initial Cu^{2+}, Ni^{2+} and Zn^{2+} ions concentration on percentage removal and adsorption capacity of ATA

5.2.8.4 Effect of Contact Time

Variation in adsorption capacity with equilibrium time has been studied at 35°C temperature, 100 mg/L initial adsorbate concentration, pH 6 and 1 g ATA dose. The results are given in Figure 5.16.

The adsorption capacity showed an increase with time and achieved equilibrium at 210 min. It was presumably due to a greater ATA surface area. The curves are smooth and continuous, which demonstrated the formation of monolayer distribution of metal ions on the outer surface of the adsorbent [315]. Ternary metal ions were removed in a certain order based on electronegativity: $Cu^{2+} > Ni^{2+} > Zn^{2+}$. Jewaratnam and Khalidi, 2019 [315] reported rapid adsorption initially due to the high availability of active sites during adsorption of Cu^{2+}, Ni^{2+} and Zn^{2+} using *Azadirachta indica* leaf powder. The number of active sites became less and ultimately all were occupied with time. Therefore, no further adsorption took place and equilibrium was reached. In the present study, similar characteristics were found in the plot. Thus, 210 minutes was optimum contact time to achieve equilibrium.

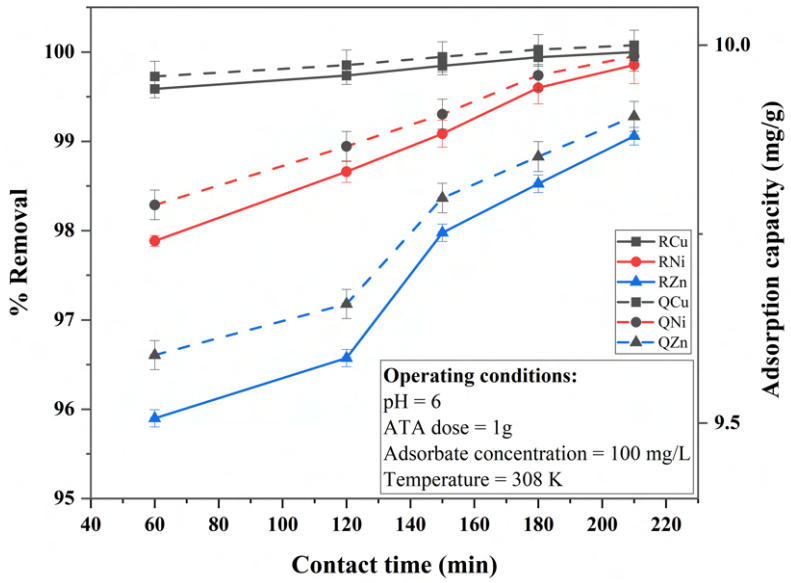

Figure 5.16: Effect of contact time on percentage removal of ternary metal ions and adsorption capacity of ATA

5.2.8.5 Effect of Temperature

The effect of temperature on the adsorption of Cu^{2+}, Ni^{2+} and Zn^{2+} ions on ATA was performed at 288, 298 and 308 K. The results are shown in Figure 5.17.

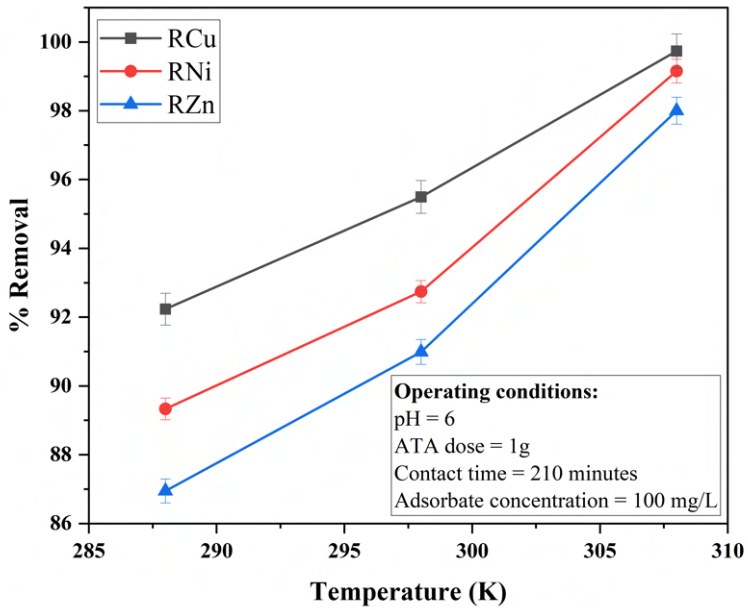

Figure 5.17: Effect of temperature on percentage removal of of ternary metal ions

The adsorption of metal ions increased with rise in temperature as showed in Figure 5.17.

It revealed that adsorption process was endothermic in nature [345]. Metal ions possessed adequate energy at higher temperature to undergo an interaction with active sites on the surface of adsorbent [346]. Moreover, the increase in temperature enhanced the rate of diffusion of the Cu^{2+}, Ni^{2+} and Zn^{2+} ions across the external boundary layer and in the internal pores of the ATA particles due to the decrement in the viscosity of the solution [347].

5.3 Adsorption mechanism for ATA

Various mechanisms including direct bonding [348], ion exchange [348], [349], surface-complex formation [348], [349], cation-π-cation interaction [350] and coordination with functional groups [351] can adsorb metal ions on ATA binding sites. Positively charged heavy metal ions get attracted towards the ATA by electrostatic attraction, which drives the adsorption. Zinc adsorption on graphene oxide is mostly driven by electrostatic attraction, according to Wang et al., 2013 [352]. A mechanism for Lead adsorption has been identified as ion exchange interactions between heavy metal ions and the proton on -OH or -COOH functional groups of adsorbent [353]. Adsorption was found to be dominated by surface complexation of heavy metal ions with oxygen-containing functional groups [354]. Ternary metal ion adsorption on ATA normally involves three basic steps: transport of metal ions from bulk solution to ATA surface, adsorption on ATA surface, and transport of metal ions within the pores of ATA particles. Likewise, ion exchange other mechanisms may be involved in the adsorption of ternary metal ions. It also includes surface complexation and electrostatic interactions.

As demonstrated in the pH optimization study, at low pH, adsorption of M^{2+} ions were significantly reduced which was attributed to high positive charge density because of protons on the surface sites, owing to competition between protons and M^{2+} ions for a limited number of adsorption sites [355]. The reduced positive charge density at the adsorption sites caused by an increase in pH, electrostatic repulsion diminishes, facilitating metal adsorption. M^{2+} ions in aqueous solution may be subjected to solvation and hydrolysis (Eqs. 5.1, 5.2 and 5.3) [356].

$$M^{2+} + nH_2O = M(H_2O)_n^{2+} \tag{5.1}$$

$$M(H_2O)_n^{2+} \rightarrow M(H_2O)^{n-1} + H^+ \tag{5.2}$$

$$nM^{2+} + mH_2O = M(OH)_m^{2n-m} + mH^+ \tag{5.3}$$

According to the Serrano et al., 1998 [357] on M^{2+} speciation, the major species is $M(OH)_2$ at pH > 6.0, while the dominant species is M^{2+} and $M(OH)^+$ at pH < 6.0. When ATA was used as an adsorbent in this investigation, the maximum removal of M^{2+} was reported at pH 5. Further rising the pH above 6 results in a decrease in adsorption, but an increase in total M^{2+} removal, which is attributed to adsorption as well as the formation of metal hydroxide, which precipitates [358], [359]. $M(OH)_2$ precipitation does not occur at a pH of 6 [360], which was determined to be ideal for adsorption. Ion exchange mechanisms that work on principle surface complex formation and the dissociation of different functional groups contained in ATA are likely to be used to explain M^{2+} ion adsorption to ATA's surface, as depicted below in Eq. 5.4 and Eq. 5.5.

$$2(-A - OH) + M^{2+} \rightarrow 2(AO)M + 2H^+ \tag{5.4}$$

$$-A - OH + M(OH)^+ \rightarrow (-AO)MOH + H^+ \tag{5.5}$$

where, 'A' denotes the matrix found in ATA

Additionally, FTIR analysis of ATA was used to determine the active functional groups involved in chemical reactions (Figure 5.4). Before and after the ternary metal ions adsorption, there were displacements in the ATA sample. Firstly, the intensity of almost all of the infrared bands appeared to decline, and the decreasing vibration intensity indicated that such material had undergone chemical changes [304]. Additionally, there were evident displacements at 2986.32 to 2978.93 cm^{-1}, 3447.60 to 3436.93 cm^{-1} and 1795.34 to 1794.21 cm^{-1} showed adsorption involves OH, NH, C=O stretching, respectively. Thus, in addition to ion exchange; solvation and complexation were also involved as the possible mechanism for adsorption od ternary metal ions on ATA.

5.4 Comparative Study

Table 5.6 shows a comparison of the adsorption capacity of ATA with other adsorbents.

Table 5.6: Comparison of different adsorbents with ATA based on adsorption capacity

Metals	Adsorbents	Biosorption capacity (mg/g)	References
Copper	Black Carrot Residue	8.88	[361]
	Luffa Acutangula Carbon	33.16	[362]
	Wheat shell	8.34	[363]
	Bone char	0.71	[364]
	Fly ash	1.08	[365]
	Sewage sludge ash	4.14	[366]
	Conocarpus pruning waste	25.36	[367]
	Nano-porous activated neem bark	16.78	[368]
	Pomelo peel	19.7	[369]
	Wheat shell (raw)	17.42	[370]
	Banana trunk	1.03	[371]
	Potato peel	1.86	[372]
	Peat	12.48	[373]
	ATA	**10.1**	**This study [374]**
Nickel	Pine bark	6.28	[375]
	Rice husk ash	4.87	[376]
	Luffa Actangula Carbon	23.84	[362]
	Bagasse fly ash	6.51	[377]
	Maple sawdust	0.294	[378]
	Expanded perlite	2.24	[379]
	Grape stalks wastes	10.68	[380]
	Tea factory waste	15.26	[381]
	Pomegranate peel	52	[382]
	Cashew nut shell (raw)	18.86	[346]
	ATA	**125**	**This study [374]**
Zinc	Nano-porous activated neem bark	21.23	[368]
	Sulfured orange peel	80	[383]
	Mango peel waste	28.21	[384]
	Agave bagasse (NaOH)	20.54	[385]
	Agave bagasse (HCL)	12.4	[385]
	Agave bagasse (HNO3)	14.43	[385]
	KCl modified orange peel	45.29	[386]
	Banana trunk	1.04	[371]

Potato peel	1.75	[372]
Canola	1.84	[372]
ATA	**3.12**	**This study [374]**

It became apparent from Table 5.6 that ATA is a good alternative for adsorption of heavy metal ions and can be used to remove Cu^{2+}, Ni^{2+} and Zn^{2+} ions from the aqueous phase.

5.5 Conclusion

The presence of 8.51% moisture, 14.78% ash, 21.49% volatile matter and 55.22% fixed carbon content were recorded in the proximate analysis of ATA. FTIR study confirmed the presence of several functional groups such as -OH, -C=O, -NH and -SO. These functional groups together with porous surface assisted in adsorbing heavy metal ions. The pH value of 6 was found to be optimal, initial concentration of 100 mg/L, contact time of 210 minutes, temperature of 308 K, and ATA dose of 1 g. A high correlation coefficient of 0.99 was found in a correlation plot of experimental and ANN predicted values, implying that a trained network was suitable for predicting adsorption. Additionally, in adsorption isotherm investigations, the Langmuir model fit better than the Freundlich and D-R models. The maximum adsorption capacity was 10.10 mg/g for Cu^{2+}, 125 mg/g for Ni^{2+} and 3.12 mg/g for Zn^{2+} by using Langmuir model parameters. Additionally, kinetics study showed supremacy of PSO model for describing the adsorption of Cu^{2+}, Ni^{2+} and Zn^{2+} ions. Results of the IPD model showed that the rate of adsorption of metal ions was controlled not only by film diffusion but also by intraparticle diffusion. The study of adsorption flux using dimensionless numbers φ (65.59, 61.51 and 60.05), N_k (27, 29 and 34) and λ (0.0002, 0.0002 and 0.0009) for Cu^{2+}, Ni^{2+} and Zn^{2+} ions, respectively demonstrated that adsorption of various metal ions on the surface of ATA was predominantly limited by diffusion, with maximal surface area coverage and decreased surface tension. Moreover, thermodynamic study indicated the endothermic and spontaneous nature of the adsorption process. The present study showed that ATA is a potential alternative for the removal of Cu^{2+}, Ni^{2+} and Zn^{2+} ions effectively from metal contaminated water.